MIT Libraries | DSpace@MIT

MIT Open Access Articles

A Method to Noninvasively Identify Cardiac Bioelectrical Sources

The MIT Faculty has made this article openly available. ***Please share*** how this access benefits you. Your story matters.

Citation: Sohn, Kwanghyun, Wener Lv, Kichang Lee, Anna Galea, Gordon Hirschman, Conor Barrett, Richard J. Cohen, and Antonis A. Armoundas. "A Method to Noninvasively Identify Cardiac Bioelectrical Sources." Pacing and Clinical Electrophysiology 37, no. 8 (August 2014): 1038–50.

As Published: http://dx.doi.org/10.1111/pace.12380

Publisher: Wiley Blackwell

Persistent URL: http://hdl.handle.net/1721.1/102578

Version: Author's final manuscript: final author's manuscript post peer review, without publisher's formatting or copy editing

Terms of use: Creative Commons Attribution-Noncommercial-Share Alike

Massachusetts Institute of Technology

NIH Public Access
Author Manuscript
Pacing Clin Electrophysiol. Author manuscript; available in PMC 2015 August 01.

Published in final edited form as:
Pacing Clin Electrophysiol. 2014 August ; 37(8): 1038–1050. doi:10.1111/pace.12380.

A Method to Noninvasively Identify Cardiac Bioelectrical Sources

KWANGHYUN SOHN, PH.D.[*], **WENER LV, M.S.**[†], **KICHANG LEE, PH.D.**[†], **ANNA GALEA, PH.D.**[‡], **GORDON HIRSCHMAN, M.ENG.**[‡], **CONOR BARRETT, M.D.**[§], **RICHARD J. COHEN, M.D., PH.D.**[†], and **ANTONIS A. ARMOUNDAS, PH.D.**[*,†]

[*]Cardiovascular Research Center, Massachusetts General Hospital, Boston, Massachusetts

[†]Institute for Medical Engineering and Science, Massachusetts Institute of Technology, Cambridge, Massachusetts

[‡]Vivonics, Inc, Waltham, Massachusetts

[§]Division of Cardiology, Cardiac Arrhythmia Service, Massachusetts General Hospital, Boston, Massachusetts

Abstract

Background—We have introduced a method to guide radiofrequency catheter ablation (RCA) procedures that estimates the location of a catheter tip used to pace the ventricles and the target site for ablation using the single equivalent moving dipole (SEMD).

Objective—To investigate the accuracy of this method in resolving epicardial and endocardial electrical sources.

Methods—Two electrode arrays, each of nine pacing electrodes at known distances from each other, sutured on the left- and right-ventricular (LV and RV) epicardial surfaces of swine, were used to pace the heart at multiple rates, while body surface potentials from 64 sites were recorded and used to estimate the SEMD location. A similar approach was followed for pacing from catheters in the LV and RV.

Results—The overall (RV & LV) error in estimating the interelectrode distance of adjacent epicardial electrodes was 0.38 ± 0.45 cm. The overall endocardial (RV & LV) interelectrode distance error, was 0.44 ± 0.26 cm. Heart rate did not significantly affect the error of the estimated SEMD location ($P > 0.05$). The guiding process error became progressively smaller as the SEMD approached an epicardial target site and close to the target, the overall absolute error was ~0.28

© 2014 Wiley Periodicals, Inc.

Address for reprints: Antonis A. Armoundas, Ph.D., Cardiovascular Research Center, Massachusetts General Hospital, 149 13th Street, Charlestown, MA 02129. Fax: 617-726-5806; aarmoundas@partners.org.

Dr. Galea is an employee of Vivonics, Inc., which has intellectual property rights in the technology reported herein.
Mr. Hirschman is majority owner of Vivonics, Inc., which has intellectual property rights in the technology reported herein.
Dr. Cohen is an inventor on university-owned patents, and/or patent applications, related to the technology reported herein
Dr. Armoundas is an inventor on university-owned patents related to the technology reported herein

Supporting Information
Additional Supporting Information may be found in the online version of this article at the publisher's website:

NIH-PA Author Manuscript
NIH-PA Author Manuscript
NIH-PA Author Manuscript

NIH-PA Author Manuscript

NIH-PA Author Manuscript

NIH-PA Author Manuscript

cm. The estimated epicardial SEMD locations preserved their topology in image space with respect to their corresponding physical location of the epicardial electrodes.

Conclusion—The proposed algorithm suggests one can efficiently and accurately resolve epicardial electrical sources without the need of an imaging modality. In addition, the error in resolving these sources is sufficient to guide RCA procedures. (PACE 2014; 37:1038–1050)

Keywords

catheter ablation; single equivalent moving dipole; noninvasive; localization; arrhythmia

Introduction

In the United States alone, approximately 785,000 people die each year from heart disease.[1] Many of these deaths are sudden and presumed to be caused by ventricular tachycardia (VT) and/or fibrillation.[1] The most common etiology of VT in the presence of infarcted tissue is the formation of a reentrant circuit, in which electrical activity circulates rapidly through and around a zone of infarction, creating a self-sustaining cycle of abnormal impulse conduction.[2] Radiofrequency catheter ablation (RCA) has been established as one of the most effective methods in treating ventricular arrhythmias.[3–7] Administration of radiofrequency current to the exit site of the reentrant circuit can permanently abolish the reentrant VT.[8,9] However, a challenging part of this treatment is the identification of the target site or recurrent VT, which ultimately requires protection by an implantable cardioverter defibrillator.

We have previously introduced an efficient and effective method in identifying the site of origin of ventricular electrical activation.[10–13] In this method, the heart's electrical activity is modeled by a single equivalent moving dipole (SEMD), the parameters of which are inversely estimated from the measured body surface potentials. While the SEMD is not a good model throughout the cardiac cycle, it provides a valid approximation of cardiac electrophysiological events when the heart's electrical activity is spatially well localized, for example, when a wave of depolarization emerges from the exit site of a reentrant circuit.[11]

In this study, we evaluate the effect of systematic and random error on the ability of our algorithm to resolve spatially separated electrical events in the heart, *in vivo*. We use multiple sites on the epicardial surface to sequentially pace the heart at different heart rates, and obtain the SEMD locations corresponding to these pacing sites from the recorded electrocardiogram (ECG) potentials. Specifically, we aim to examine the hypothesis that the algorithm we developed to obtain the SEMD parameters from body surface ECG signals is robust in identifying spatially separated electrical events at different heart rates while maintaining in image space the same topology with that in real space.

Methods

Animal Studies

We evaluated the applicability of a recently developed algorithm to identify the SEMD parameters, and the ability of that model to represent cardiac electrical activity, in a swine

NIH-PA Author Manuscript

NIH-PA Author Manuscript

NIH-PA Author Manuscript

animal model. The experimental protocol was approved by the MIT Committee on Animal Care. We performed 18 swine studies. Thirteen swine were used for epicardial pacing and weight, radius, and length of the pigs were 39.2 ± 4.3 kg, 14.8 ± 1.2 cm, and 59.4 ± 1.6 cm, respectively. Five swine were used for endocardial pacing and weight, radius, and length of the pigs were 44.8 ± 1.0 kg, 17.0 ± 0.0 cm, and 60.0 ± 0.0 cm.

The surgical preparation for the epicardial pacing studies has been described previously.[11,12] Briefly, following sternotomy, a linear electrode array was sutured on the epicardial surface of the right ventricle longitudinally from apex to base direction. And, another electrode array was also sutured on the left ventricle in the same way. There were nine electrodes on each electrode array. Electrodes on the right array were named A1–A9, from apex side electrode to base side one. Electrodes on the left array were also named B1–B9 in the same way. Interelectrode distances of A1–A2 and B1–B2 were 2 mm, and all other adjacent electrode distances were 10 mm. The electrode cables were passed subcutaneously through an intercostal space to the cranoiolateral thorax, exteriorized and fixed by stay sutures. The chest was closed in layers, and air evacuated from the chest. At all times the animals were monitored using ECG, pulse oximetry, blood pressure, and body temperature. We paced the heart from a stimulus generator (STG2008, Multi Channel Systems, Reutlingen, Germany) that delivered pacing pulses of duration 1 ms and amplitude 3 mA between individual bipolar electrodes, at 120, 140, 160, 180, 200, and 220 beats/min. At the conclusion of the experiment the exact coordinates of the heart boundaries, as well as the epicardial electrodes on the right and left ventricles, were determined.

For the endocardial pacing studies, two ablation catheters were introduced into the pig's heart: a catheter with five bipolar electrodes in the right ventricle and a catheter with 10 bipolar electrodes in the left ventricle; the interelectrode distance between bipolar electrodes was 12 mm. Similarly, pacing pulses were applied to the bipolar electrodes at 120, 140, 160, 180, and 200 beats/min as far as stable pacing was achievable.

Sixty-four recording electrodes were placed on the torso to measure body surface potentials. Eight electrodes were evenly placed on a single electrode strip, and eight electrode strips were used for this study. Interelectrode distance between adjacent electrodes on an array was 4.5 cm. Each electrode strip was aligned longitudinally to the torso. Two electrode strips were positioned on the left and right lateral posterior regions, two others on the left and right lateral sides, two others on the left and right lateral anterior regions, and the last two were placed on the left and right anterior torso.

The ECG acquisition system included a high-fidelity BioSemi amplifiers (Active Two, BioSemi, Amsterdam, the Netherlands), a very flexible, 24-bit, true DC, battery-powered front-end, with fiber optic data transfer system, which allowed the recording of 64 body-surface potentials that were digitized at 8,192 Hz (Labview, National Instrument Corp., Austin, TX, USA). Data were analyzed off-line using custom-built software.

The Algorithm for the Inverse-Problem Estimation

In the inverse algorithm, we used the SEMD model embedded in an infinite homogeneous volume conductor.[10,11] Then, the potential φ^j at location $\mathbf{r}^i$ (x^i, y^i, z^i) on the body surface

NIH-PA Author Manuscript

NIH-PA Author Manuscript

NIH-PA Author Manuscript

due to the dipole at $\mathbf{r}'$ (x′, y′, z′) with moment $\mathbf{p}$ (p_x, p_y, p_z), in an infinite medium of conductivity g, were given by

$$\Phi^i(\mathbf{r}', \mathbf{p}) = \frac{1}{4\pi g} \frac{\mathbf{p} \bullet (\mathbf{r}^i - r')}{|\mathbf{r}^i - \mathbf{r}'|^3}. \quad (1)$$

The ($\mathbf{r}'$, $\mathbf{p}$) estimates were obtained by the Simplex method[14] that minimized sum of the squares of differences between measured and calculated potentials:

$$\psi = \sum_{i=1}^{I} (\phi^i - \phi_m^i)^2, \quad (2)$$

where ϕ^i_m was the measured body surface potential at location i due to the bioelectric source, and I was the number of electrodes.[11,12]

Briefly, the algorithm search started from random seeds (distributed in a volume approximately representing the heart) that represented the SEMD initial location and this process repeated a maximum of 10 times. A spatial criterion was imposed to force solutions to land inside a predefined volume that includes the heart.[10–12,15] In prior studies[11,12] we have determined that the algorithm is convergent to a global minimum and hence terminated, if two solutions that start from two different seeds are found to be closer than 0.2 cm. Therefore, if after 10 seeds there were no solutions that satisfied the spatial criterion and were closer than 0.2 cm apart, the algorithm outcome was considered to be nonconvergent.

Data Processing

In offline analysis, each of the surface ECG channels was visually inspected to ensure good data quality, and all body surface potentials were referenced to the average of the 64 body surface potentials. Then, the R-wave of each QRS complex was identified for all channels. The baseline of each beat was subsequently adjusted relative to an isoelectric segment preceding the pacing spike.

However, because at fast heart rates the pacing spike tended to be close or overlap with the previous T-wave and therefore the segment preceding the pacing spike was not isoelectric anymore, at heart rates greater than 180 beats per minute (bpm), we employed a method (see Supporting Online Information) in which the average potential over the whole beat was used for baseline adjustment. After ECG complexes were identified, an iterative, adaptive QRS template matching scheme was used to refine initial fiducial point estimates.[16] Next, a median beat was computed for each ECG lead by aligning each beat within the lead data segment according to the R-wave and identifying the median value on a point-by-point basis within the beat.

After estimation of the median beat for each channel, a noise estimate was obtained from each median beat by measuring the standard deviation of the signal fluctuations in a predefined isoelectric segment that preceded the pacing spike.

NIH-PA Author Manuscript

NIH-PA Author Manuscript

NIH-PA Author Manuscript

Ideally, the best time for the estimation of the pacing electrode location is the initial moment of activation. However, practically, one needs to employ a time moment when the signal-to-noise ratio (SNR) is high enough to apply the above-mentioned inverse algorithm. Therefore, we considered the SEMD location at the earliest activation time (EAT) to correspond with the estimated pacing electrode location.[17–20] To determine the EAT, we have considered the activation time at each body surface electrode defined as the time instant of the maximum potential change in 2.3 ms from the beginning up to the peak of the QRS complex, either increase or decrease; then, the EAT is determined as the earliest time among the activation times of the 64 electrodes.

Optimization Algorithm and Statistical Criteria

We used Matlab (MathWorks, Natick, MA, USA) function "*fminsearch*," that implements the Simplex method, to estimate the SEMD location by minimizing ψ. Since measurement noise can generate uncertainty of the estimated dipole parameters, we adopted the prediction error theory[21,22] to estimate confidence intervals of each of the SEMD parameters as described by Armoundas et al.[12] Especially in this report, "prediction error" represents uncertainty level of estimated dipole location due to measurement error and defined, as

$$\sigma^{\mathrm{pr}}=\sqrt{(\sigma_{\mathrm{x}}^{\mathrm{pr}})^2+(\sigma_{\mathrm{y}}^{\mathrm{pr}})^2+(\sigma_{\mathrm{z}}^{\mathrm{pr}})^2}, \quad (3)$$

where $\sigma_{\mathrm{x}}^{\mathrm{pr}}$, $\sigma_{\mathrm{y}}^{\mathrm{pr}}$, and $\sigma_{\mathrm{z}}^{\mathrm{pr}}$ are standard deviations of estimated locations in x, y, and z coordinates, respectively.

We have also defined SNR at each instant of the cardiac cycle as

$$\mathrm{SNR}=10\log_{10}\left(\frac{1}{\mathrm{I}}\sum_{\mathrm{i}=1}^{\mathrm{I}}\left(\frac{\phi_{\mathrm{i}}}{\sigma_{\mathrm{i}}}\right)^2\right), \quad (4)$$

where I is the number of body surface electrodes, and φ_{i} and σ_{i} are potential and noise standard deviation of ith electrode, respectively.

Results

We employed ECG data recorded during pacing from nine different epicardial locations (A1 to A9) on the right ventricle and another nine locations (B1 to B9) on the left ventricle to estimate the SEMD at EAT.

Accuracy of the Estimated Epicardial Pacing Electrode Locations

We first sought to examine the ability of the algorithm to accurately localize each of the nine epicardial electrodes on the right and left ventricles. Figure 1 shows the distance between the real pacing electrode locations and the estimated ones, at EAT. The results from pacing electrodes A1–A9 are displayed in Figure 1(A) and pacing electrodes B1–B9 are displayed in Figure 1(B). The bar-plots for each electrode represent the distance between the real location and the estimated location at six different heart rates, from 120 bpm to 220 bpm. Each bar-plot is derived from the distribution of the real minus the estimated pacing

NIH-PA Author Manuscript

NIH-PA Author Manuscript

NIH-PA Author Manuscript

electrode locations corresponding to each heart rate and pacing electrode. The median values of the real minus the estimated pacing electrode locations range between 2 cm and 4 cm, and the standard deviation of these distances range between 0.5 cm and 2 cm.

Analysis of variance (ANOVA) indicated that there are no statistical differences for the distances between the real and the estimated pacing electrode locations, as a function of heart rate. There are no statistical differences in the distance between adjacent electrodes except A3/A4 and B2/B3 pairs ($P < 0.05$). The overall distance between the real and the estimated pacing electrode locations was not different between the right and left ventricles except A3/B3 pair ($P < 0.05$).

If we consider all animals, heart rates, and pacing electrodes, the average distance between the real and the estimated pacing electrode locations is 2.76 ± 1.14 cm. To probe the validity of the choice of EAT, we estimated the time interval of the EAT from the pacing spike time (PST) across the same recordings and we found it to be 37.6 ± 8.6 ms. Interestingly, assuming a propagation velocity of ~50 cm/s, a wavefront in 37.6 ms would travel ~1.88 cm, a distance that is in agreement with the distance obtained for the SEMD locations at EAT (2.76 ± 1.14 cm).

It should be noted that the results described include both components of the error: systematic error (due to the inverse model selection) and random error (due to measurement noise).

Variation of the Estimated SEMD Locations due to Measurement Noise

Having estimated the distance that the SEMD propagates from the PST to the EAT, we sought to examine the contribution of the random error in the estimated SEMD location compared to the true one.

Given that in the intended application of this method the systematic error when trying to superpose the SEMD due to the catheter tip to the SEMD corresponding to the site of the arrhythmia is expected to cancel out, one needs to know the uncertainty in the SEMD location due to random noise. In that case, one can compute the uncertainty of the dipole parameters by adding different noise realizations to experimental data and measuring the resulting distribution of the dipole parameters. However, this method is time consuming and not suitable for a real-time application. Here we employ the concept of the prediction error[12] to estimate the predicted uncertainty of the SEMD spatial parameters due to measurement noise.

Figure 2 displays representative traces of the prediction error and SNR during the cardiac cycle. One observes that the prediction error in large during the period from the end of the T wave until the pacing spike, when SNR is low. Then, the prediction error takes its minimum value close to the peak of the QRS complex, when SNR is a maximum. The prediction error increases during the terminal portion of the QRS as the activation front becomes spatially distributed, and remains relatively constant during the ST-segment and T wave. Overall, larger body surface potentials lead to larger SNR and smaller prediction error.

To examine whether the error due to measurement noise changes as the heart rate increases we sought to examine the prediction error at the EAT at different heart rates (Fig. 3). Results

NIH-PA Author Manuscript

NIH-PA Author Manuscript

NIH-PA Author Manuscript

from pacing sites at the right ventricle (A1–A9) and at the left ventricle (B1–B9) are presented in Figures 3(A) and 3(B), respectively. There are no statistical differences (ANOVA) of the prediction error distributions as a function of heart rate for each of the pacing electrodes in the right and left ventricles.

From a biophysical point of view, the earlier the EAT detection occurs during the cardiac cycle, the smaller the size of the depolarized tissue and the better the representation of this depolarized tissue with an SEMD. However, in order to better localize the SEMD, the SNR has to increase enough, such that the uncertainty of the SEMD location gets minimized. Therefore, the earlier in the cardiac cycle the SEMD is identified the smaller the SNR and the larger the prediction error.

In order to obtain an optimal relationship between the SNR and the prediction error in Figure 4, we plot the relationship between the prediction error and SNR for solutions ranging from 4 ms after the pacing spike to the QRS peak (data points are obtained from all swine and all pacing electrodes in the right and left ventricles, for all heart rates). One observes that the prediction error follows an inverse relation to SNR (prediction error = $1.08 \times \exp(-0.11 \times \text{SNR})$, $R = 0.98$). As the depolarization wavefront propagates away from the pacing electrode site the prediction error decreases but SNR increases.

Overall, Figures 2 and 3 indicate that the error due to the measurement noise is mostly less than 0.01 cm at EAT, and for SNR values ranging from 5% to 95% at EAT, the 5–95% prediction error values are 0.002 cm and 0.012 cm, respectively; these values are very small and suitable for the intended use of this algorithm in guiding the tip of the ablation catheter to the site of the origin of the arrhythmia.

Accuracy of the Estimated Distance between Neighboring Epicardial Pacing Electrodes

We then sought to determine the heart-rate-dependent ability of the algorithm to resolve spatially separated electrical events in the heart, or alternatively to examine the contribution of the systematic error in the estimated SEMD location.

In Figure 5, we examine the ability of our algorithm in determining the separation distance of the epicardial pacing electrodes in the right (A1–A9) and left ventricles (B1–B9). We chose to present only the difference of neighboring electrodes to reduce the confounding error resulting from the systematic error due to the curvature of the heart.

The distance between A1 and A2 and between B1 and B2 is 0.2 cm, while all other interelectrode distances are 1 cm. When all heart rates are considered together, A1A2 interelectrode distance has been estimated to be 0.28 ± 0.26 cm, while the interelectrode distance of the remaining electrodes in the right ventricle has been estimated to be 0.74 ± 0.55 cm. Similarly, in the left ventricle, B1B2 interelectrode distance has been estimated to be 0.34 ± 0.34 cm, while the remaining interelectrode distance has been estimated to be 0.92 ± 0.80 cm. ANOVA indicates that there are no statistical differences in the estimated interelectrode distances as a function of heart rate for either ventricle. Also, there is no statistical difference in the estimated interelectrode distances between left and right ventricle

NIH-PA Author Manuscript

NIH-PA Author Manuscript

NIH-PA Author Manuscript

($P > 0.05$). The overall interelectrode distance error is 0.37 ± 0.35 cm in the right ventricle and 0.39 ± 0.59 cm in the left ventricle.

Therefore, it appears that irrespective of the heart rate the proposed algorithm is capable in resolving spatially separated electrical events in the heart, with the accuracy required in the intended application, suggesting that the systematic error is likely to have a minor effect when trying to superpose the ablation catheter to the site of origin of the arrhythmia.

Accuracy of the Estimated Distance between Neighboring Endocardial Pacing Electrodes

We then sought to determine the heart-rate-dependent ability of the algorithm to resolve spatially separated electrical events at the endocardial surface of the heart, or alternatively to examine whether the contribution of the systematic error in the estimated SEMD location, is different in the right-ventricular (RV) versus left-ventricular (LV) as well as in the endocardial versus epicardial surface.

Endocardial pacing using multipole ablation catheters were used in three animals. A catheter with five dipole pacing electrodes was introduced in the RV and a catheter with 10 dipole pacing electrodes was introduced in the LV. The distance between each of the two pacing poles was 3 mm, while the distance between adjacent pacing electrodes was 1.2 cm. The hearts were paced at 120, 140, 160, 180, and 200 bpm.

Since the actual catheter lead locations in the RV and LV could not be measured, Figure 6 shows the interelectrode distance estimated from the endocardial pacing sites. When all heart rates are considered together, the estimated distance is 0.47 ± 0.52 cm in the RV ($n = 13$), 1.00 ± 0.41 cm in the LV ($n = 42$), and 0.80 ± 0.47 cm in both ventricles combined. ANOVA indicates that there is no statistically significant difference across the estimated distances as a function of heart rate, for either ventricle ($P = 0.518$ in the RV and $P = 0.893$ in the LV). But, the estimated interelectrode distance is different between the LV and RV ($P = 0.003$). Finally, the overall interelectrode distance error is 0.76 ± 0.23 cm in the RV and 0.40 ± 0.21 cm in the LV, while the combined endocardial interelectrode distance error in RV and LV is 0.44 ± 0.26 cm.

Finally, we evaluated the statistical difference of the errors between the endocardial pacing from multipole catheters and the epicardial pacing with sutured electrode arrays. While there is no significant difference of the errors between endocardial and epicardial pacing leads in the LV ($P = 0.089$), there is a statistically significant difference between endocardial and epicardial pacing leads in the RV ($P = 0.001$).

Relationship of Relative and Absolute Error

We have observed that the systematic error causes a significant offset of the estimated compared to the true pacing electrode location (Fig. 1). However, since in the intended application our goal is to superpose the dipole due to the catheter tip to the dipole due to the site of origin of the arrhythmia, we have hypothesized that as the SEMD due to the catheter tip approaches the SEMD due to the site of origin of the arrhythmia, the systematic error will progressively have the same effect to each SEMD localization.[11,15,23–25]

NIH-PA Author Manuscript

NIH-PA Author Manuscript

NIH-PA Author Manuscript

To further investigate this hypothesis, we have plotted the relative and absolute errors between the estimated pacing electrode locations (Fig. 7). We used all neighboring pacing electrode combinations in the right (A_i/A_j, $i \neq j$) and left (B_i/B_j, $i \neq j$) ventricles and let A_i and B_i be the SEMD locations due to the catheter and A_j and B_j be the SEMD locations due to the target. In Figure 7, subscripts "t" and "e" indicate the true and estimated dipole locations, respectively. The absolute error is defined as the estimated distance between two pacing electrodes, while the relative error is defined as the ratio of two pacing electrode localization errors.

Figures 7(A) and 7(B) show the relative error versus the real distance in the right and left ventricle, respectively, across all animals and all pacing rates. One observes that the relative errors either in the right or the left ventricle approach 1 as the real distance decreases. This result suggests that superposition of two estimated SEMD locations in image space would lead to superposition of the SEMD sources in real space. In Figures 7(C) and 7(D), the absolute error plots in the right and left ventricles, respectively, indeed support the concept that as the estimated distance between the locations of two SEMD sources becomes smaller, so does the distance of the SEMD locations in real space. Overall, these results present the first experimental evidence that the systematic error does not hinder the ability to guide the catheter tip to the target site.

Evaluation of the Uniqueness of the SEMD Solutions

A very important property of an algorithm aimed to help guide the tip of the catheter to the ablation site should be its "directionality" or in other words its ability to exclusively guide the tip to the target site. One way to answer this question is by examining whether the relative location of the estimated dipole with respect to the true dipole location is maintained or otherwise whether the topology of the true dipole locations in the ventricle is conserved and reproduced by the locations of the SEMDs.

In Figure 8, we plot the 3D distribution of the estimated pacing electrode locations, across all animals and all pacing rates. The center of each ellipsoid reflects the estimated median pacing electrode location across all animals, while the semiaxis reflects the standard error in that direction. Interestingly, despite the inhomogeneous systematic error, the estimated distributions of the pacing electrode locations follow a trajectory that agrees with the physical order of the electrodes on the epicardial surface. These results suggest that despite differences in the systematic error across the left and right ventricles, the proposed algorithm has been able to resolve the topology of the pacing electrodes either in the right or the left ventricle, suggesting that it could also uniquely guide the catheter tip toward the ablation site.

Discussion

The most common etiology of VT in the presence of myocardial infarction is the formation of reentrant circuit. Delivery of radiofrequency current to the exit site of the reentrant circuit remains the most successful approach to eliminate the reentrant VT.[4,6] However, the most challenging aspect of this treatment option is the identification of the exit site.[26,27] The selection of the appropriate ablation site is achieved by painstaking mapping of the electrical

NIH-PA Author Manuscript

NIH-PA Author Manuscript

NIH-PA Author Manuscript

activity on the endocardial surface of the heart and often, this recording must be done while the arrhythmia is ongoing.

The CARTO™ (Biosense Webster, Diamond Bar, CA, USA) system has been an established method that provides an electro-anatomical map of the heart. The basic assumption of this method is that the activation pattern and chamber geometry are constant from beat to beat. However, multiple morphologies of VT are common in patients with scar-related VT. Thus, monitoring of the activation sequence of the ongoing arrhythmia[27,28] has resulted in a success rate of terminating the target VT of 82%, while when targeting all inducible monomorphic VTs the complete procedural success was 64-. An alternative to the CARTO system has been the Ensite (St. Jude Medical, St. Paul, MN, USA) system that employs a noncontact 64-electrode basket catheter that is placed inside the heart. However, the movement of the heart during systole is not taken into account, which might limit the clinical applicability of this system in patients with large cardiac chambers, or it could require balloon repositioning to the areas of interest.[29] New cardiac imaging techniques,[30] by magnetic resonance imaging,[31–33] computed tomography,[34–36] or ultrasound,[37] have been introduced to overcome limitations mentioned above. However, the acquisition of 3D anatomical information and corresponding inverse solutions makes them particularly time consuming.

To overcome these challenges, we have developed a method that models cardiac electrical activity with an SEMD, and we have performed a detailed evaluation in a swine animal model of the ability of this method to accurately identify the location of the SEMD. Specifically, we have shown that under realistic conditions, the algorithm we have used to identify the SEMD location corresponding to epicardial and endocardial pacing sites, first, achieves rapid convergence to a global minimum; second, the systematic error has minimal effect in accurately identifying the epicardial pacing sites; third, although the homogeneous volume conductor introduces systematic error in the estimated compared to the true dipole location, we find that the interelectrode distance error is small for epicardial (0.37 ± 0.35 cm in the RV and 0.39 ± 0.59 cm in the LV) and endocardial (0.76 ± 0.23 cm in the RV and 0.40 ± 0.21 cm in the LV) sites, and suitable to guide catheter ablation procedures; fourth, the error in the guiding process becomes progressively smaller as one approaches the target site, and close to the target the overall absolute error becomes ~0.28 cm, that is appropriate for RCA procedures; fifth, the relative location of the estimated dipoles with respect to the true dipole sources is maintained, thus ensuring the inverse algorithm conserves the topology of the source distribution employed in the forward problem, a finding that has significant implications in guiding RCA procedures; sixth, the algorithm does not require preacquired spatial anatomical information to determine cardiac sources of activation.

The results of this study further suggest that, at least in this setting, the algorithm to estimate the SEMD location corresponding to epicardial or endocardial sites is not sensitive to electrophysiological (i.e., overlap of the repolarization phase of the preceding beat to the depolarization phase of the current beat) and/or mechanical (i.e., movement of the heart) factors, resulting from high heart rates.

NIH-PA Author Manuscript

NIH-PA Author Manuscript

NIH-PA Author Manuscript

The proposed algorithm uses a simple model to represent cardiac electrical activity. The choice of fitting the SEMD to potentials at EAT, as the time instant during the cardiac cycle that would be suitable for ablation, is based on the idea that the depolarization wavefront during VT will be close to the exit and thus well localized, but also large enough to give rise to potentials that exceed the noise level. In this approach, the use of the infinite homogeneous volume conductor model is expected to introduce considerable systematic error in localizing a bioelectrical source. In this study, we have seen that the overall error in estimating the epicardial pacing site locations is 2.76 ± 1.14 cm, while the overall error in estimating the distance of adjacent pacing electrode locations is 0.38 ± 0.45 cm. Similarly, for endocardial sites the overall error in estimating the distance of adjacent pacing electrode locations is 0.44 ± 0.26 cm. These errors are an order of magnitude smaller than the pacing electrode localization error, and appropriate for this application.

While systematic error (due to lack of realistic anatomic geometry) is expected to affect the estimation of the SEMD corresponding to the arrhythmic focus and the SEMD of the catheter tip precisely in the same way when the two are superposed, this may not occur if the two SEMDs have different dipole orientations and may also not occur if superposition cannot be achieved (e.g., when the source is intramural or epicardial and the catheter tip is restricted to the endocardial surface). Prior computer simulations suggest that the contribution of dipole orientation to noncanceling error is small (~0.04 cm).[11] Finally, the fact that we were able to estimate the separation of adjacent electrodes without knowing their precise orientation suggests that if full superposition is not achieved, the relative locations are still estimated accurately.

Further support to this claim is provided by Figures 7(A) and 7(B), which suggest that as the real distance between two epicardial sources becomes smaller, the localization error of the two sources becomes identical. In addition, in Figures 7(C) and 7(D), one observes that as the real distance between the epicardial sources decreases, so does their distance in image space. It is also worth mentioning that in Figures 7(C) and 7(D) the estimated distances are in general smaller than the true distances. This might be due to the curvature of the heart, in which case the physical distance between two pacing electrodes is smaller than their distance on the epicardial surface.

Finally, an important aspect of the clinical applicability of this technology relates to whether the real space topology is maintained in the image space. In Figure 8, the relative locations of pacing electrodes are well maintained in the image space. This supports the idea that the superposition of SEMDs in the image space leads to the superposition of corresponding current sources in the real space. Or alternatively, if we guide the SEMD due to the catheter tip to the SEMD due to the target site, then the catheter tip in real space will be superposed with the target site in real space.

In summary, in this manuscript we systematically evaluate an algorithm aiming to provide a reliable, accurate, and fast means in guiding the ablation catheter to the site of the origin of the arrhythmia. Our approach is based on the principle that for many arrhythmias, the electrical activity within the heart is highly localized for a portion of the cardiac cycle. If one can localize the site of origin of the arrhythmia during the cardiac cycle then one can ablate

NIH-PA Author Manuscript

NIH-PA Author Manuscript

NIH-PA Author Manuscript

it. The proposed method here ignores boundary conditions and inhomogeneities in tissue conductivity. However, we have shown that as long as the site of origin of the arrhythmia and the tip of the catheter are identified using the same algorithm, then when the two are brought together, both their positions will be distorted by the same amount. In other words, when the algorithm identifies that the site of the origin of the arrhythmia and catheter tip are at the same location, then they are at the same location. Thus the distortion due to the above factors should not significantly affect the accuracy to which one can make the tip of the ablation catheter and site of origin of the arrhythmia coincide.

Supplementary Material

Refer to Web version on PubMed Central for supplementary material.

Acknowledgments

The work was supported by NIH grants 1RO1HL103961 and R44 HL079726-04.

References

1. Go AS, Mozaffarian D, Roger VL, Benjamin EJ, Berry JD, Borden WB, Bravata DM, et al. Executive summary: Heart disease and stroke statistics—2013 update: A report from the American Heart Association. Circulation. 2013; 127:143–152. [PubMed: 23283859]
2. Zipes DP, Wellens HJ. What have we learned about cardiac arrhythmias? Circulation. 2000; 102:IV52–IV57. [PubMed: 11080132]
3. Stevenson WG, Delacretaz E. Strategies for catheter ablation of scar-related ventricular tachycardia. Curr Cardiol Rep. 2000; 2:537–544. [PubMed: 11060581]
4. Stevenson WG, Delacretaz E. Radiofrequency catheter ablation of ventricular tachycardia. Heart. 2000; 84:553–559. [PubMed: 11040021]
5. Delacretaz E, Soejima K, Stevenson WG, Friedman PL. Short ventriculoatrial intervals during orthodromic atrioventricular reciprocating tachycardia: What is the mechanism? J Cardiovasc Electrophysiol. 2000; 11:121–124. [PubMed: 10695474]
6. Stevenson WG, Friedman PL, Kocovic D, Sager PT, Saxon LA, Pavri B. Radiofrequency catheter ablation of ventricular tachycardia after myocardial infarction. Circulation. 1998; 98:308–314. [PubMed: 9711935]
7. Calkins H, Epstein A, Packer D, Arria AM, Hummel J, Gilligan DM, Trusso J, et al. Catheter ablation of ventricular tachycardia in patients with structural heart disease using cooled radiofrequency energy: Results of a prospective multicenter study. Cooled RF Multi Center Investigators Group. J Am Coll Cardiol. 2000; 35:1905–1914. [PubMed: 10841242]
8. Delacretaz E, Stevenson WG. Catheter ablation of ventricular tachycardia in patients with coronary heart disease. Part II: Clinical aspects, limitations, and recent developments. Pacing Clin Electrophysiol. 2001; 24:1403–1411. [PubMed: 11584464]
9. Delacretaz E, Stevenson WG. Catheter ablation of ventricular tachycardia in patients with coronary heart disease: Part I: Mapping. Pacing Clin Electrophysiol. 2001; 24:1261–1277. [PubMed: 11523613]
10. Armoundas AA, Feldman AB, Sherman DA, Cohen RJ. Applicability of the single equivalent point dipole model to represent a spatially distributed bio-electrical source. Med Biol Eng Comput. 2001; 39:562–570. [PubMed: 11712653]
11. Armoundas AA, Feldman AB, Mukkamala R, Cohen RJ. A single equivalent moving dipole model: An efficient approach for localizing sites of origin of ventricular electrical activation. Ann Biomed Eng. 2003; 31:564–576. [PubMed: 12757200]

NIH-PA Author Manuscript NIH-PA Author Manuscript NIH-PA Author Manuscript

12. Armoundas AA, Feldman AB, Mukkamala R, He B, Mullen TJ, Belk PA, Lee YZ, et al. Statistical accuracy of a moving equivalent dipole method to identify sites of origin of cardiac electrical activation. IEEE Trans Biomed Eng. 2003; 50:1360–1370. [PubMed: 14656065]
13. Lee K, Lv W, Ter-Ovanesyan E, Barley ME, Voysey GE, Galea AM, Hirschman GB, et al. Cardiac ablation catheter guidance by means of a single equivalent moving dipole inverse algorithm. Pacing Clin Electrophysiol. 2013; 36:811–822. [PubMed: 23448231]
14. Nelder JA, Mead R. A Simplex method for function minimization. Comput J. 1965; 7:308–313.
15. Fukuoka Y, Oostendorp TF, Sherman DA, Armoundas AA. Applicability of the single equivalent moving dipole model in an infinite homogeneous medium to identify cardiac electrical sources: A computer simulation study in a realistic anatomic geometry torso model. IEEE Trans Biomed Eng. 2006; 53:2436–2444. [PubMed: 17153200]
16. Smith JM, Clancy EA, Valeri CR, Ruskin JN, Cohen RJ. Electrical alternans and cardiac electrical instability. Circulation. 1988; 77:110–121. [PubMed: 3335062]
17. Blanchard SM, Smith WM, Damiano RJ Jr, Molter DW, Ideker RE, Lowe JE. Four digital algorithms for activation detection from unipolar epicardial electrograms. IEEE Trans Biomed Eng. 1989; 36:256–261. [PubMed: 2917771]
18. Gepstein L, Hayam G, Ben-Haim SA. Activation-repolarization coupling in the normal swine endocardium. Circulation. 1997; 96:4036–4043. [PubMed: 9403629]
19. Paul T, Moak JP, Morris C, Garson A Jr. Epicardial mapping: How to measure local activation? Pacing Clin Electrophysiol. 1990; 13:285–292. [PubMed: 1690401]
20. Rosenbaum DS, Wilber DJ, Smith JM, Du D, Ruskin JN, Garan H. Local activation variability during monomorphic ventricular tachycardia in the dog. Cardiovasc Res. 1992; 26:237–243. [PubMed: 1423418]
21. Ljung, L. Asymptotic distribution of parameter estimates. In: Kailath, T., editor. System Identification: Theory for the User. Englewood Cliffs, NJ: PTR Prentice Hall Information and System Sciences; 1987. p. 240-243.
22. Bard, Y. Interpretation of the Estimates. New York: Academic Press; 1974.
23. Barley ME, Armoundas AA, Cohen RJ. A method for guiding ablation catheters to arrhythmogenic sites using body surface electrocardiographic signals. IEEE Trans Biomed Eng. 2009; 56:810–819. [PubMed: 19272900]
24. Barley ME, Choppy KJ, Galea AM, Armoundas AA, Rosbury TS, Hirschman GB, Cohen RJ. Validation of a novel catheter guiding method for the ablative therapy of ventricular tachycardia in a phantom model. IEEE Trans Biomed Eng. 2009; 56:907–910. [PubMed: 19272901]
25. Fukuoka Y, Oostendorp TF, Armoundas AA. Method for guiding the ablation catheter to the ablation site: A simulation and experimental study. Med Biol Eng Comput. 2009; 47:267–278. [PubMed: 19194733]
26. Stevenson WG, Sager PT, Natterson PD, Saxon LA, Middlekauff HR, Wiener I. Relation of pace mapping QRS configuration and conduction delay to ventricular tachycardia reentry circuits in human infarct scars. J Am Coll Cardiol. 1995; 26:481–488. [PubMed: 7608454]
27. Nademanee K, Kosar EM. A nonfluoroscopic catheter-based mapping technique to ablate focal ventricular tachycardia. Pacing Clin Electrophysiol. 1998; 21:1442–1447. [PubMed: 9670189]
28. Stevenson WG, Delacretaz E, Friedman PL, Ellison KE. Identification and ablation of macroreentrant ventricular tachycardia with the CARTO electroanatomical mapping system. Pacing Clin Electrophysiol. 1998; 21:1448–1456. [PubMed: 9670190]
29. Okishige K, Kawabata M, Umayahara S, Yamashiro K, Gotoh M, Isobe M, Strickberger SA. Radiofrequency catheter ablation of various kinds of arrhythmias guided by virtual electrograms using a noncontact, computerized mapping system. Circ J. 2003; 67:455–460. [PubMed: 12736487]
30. Wang Y, Cuculich PS, Zhang J, Desouza KA, Vijayakumar R, Chen J, Faddis MN, et al. Noninvasive electroanatomic mapping of human ventricular arrhythmias with electrocardiographic imaging. Sci Transl Med. 2011; 3:98ra84.
31. Berger T, Fischer G, Pfeifer B, Modre R, Hanser F, Trieb T, Roithinger FX, et al. Single-beat noninvasive imaging of cardiac electrophysiology of ventricular pre-excitation. J Am Coll Cardiol. 2006; 48:2045–2052. [PubMed: 17112994]

NIH-PA Author Manuscript

NIH-PA Author Manuscript

NIH-PA Author Manuscript

32. Modre R, Tilg B, Fischer G, Hanser F, Messnarz B, Seger M, Schocke MF, et al. Atrial noninvasive activation mapping of paced rhythm data. J Cardiovasc Electrophysiol. 2003; 14:712–719. [PubMed: 12930250]

33. Smith NP, Buist ML, Pullan AJ. Altered T wave dynamics in a contracting cardiac model. J Cardiovasc Electrophysiol. 2003; 14:S203–S209. [PubMed: 14760925]

34. Ramanathan C, Ghanem RN, Jia P, Ryu K, Rudy Y. Noninvasive electrocardiographic imaging for cardiac electrophysiology and arrhythmia. Nat Med. 2004; 10:422–428. [PubMed: 15034569]

35. Ramanathan C, Jia P, Ghanem R, Ryu K, Rudy Y. Activation and repolarization of the normal human heart under complete physiological conditions. Proc Natl Acad Sci U S A. 2006; 103:6309–6314. [PubMed: 16606830]

36. Zhang X, Ramachandra I, Liu Z, Muneer B, Pogwizd SM, He B. Noninvasive three-dimensional electrocardiographic imaging of ventricular activation sequence. Am J Physiol Heart Circ Physiol. 2005; 289:H2724–H2732. [PubMed: 16085677]

37. Cheng LK, Sands GB, French RL, Withy SJ, Wong SP, Legget ME, Smith WM, et al. Rapid construction of a patient-specific torso model from 3D ultrasound for non-invasive imaging of cardiac electrophysiology. Med Biol Eng Comput. 2005; 43:325–330. [PubMed: 16035219]

NIH-PA Author Manuscript

NIH-PA Author Manuscript

NIH-PA Author Manuscript

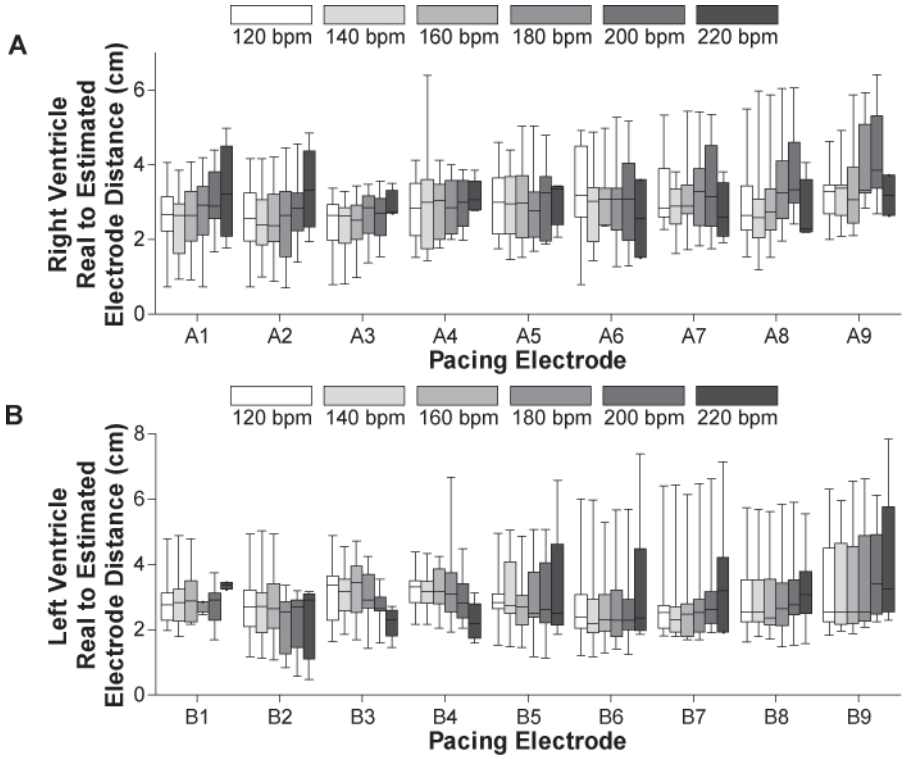

Figure 1.

Distance between the real pacing spike location and the estimated single equivalent moving dipole location calculated at the earliest activation time. Results from pacing sites at the right (A1–A9) and left ventricles (B1–B9) are presented at the first and the second entries, respectively. At each electrode, the distances at different heart rates are displayed separately. For each intervention, the median (horizontal solid line), 75–25% percentiles (box), and 95–5% percentiles (error bars) are shown. bpm = beats per minute.

NIH-PA Author Manuscript
NIH-PA Author Manuscript
NIH-PA Author Manuscript

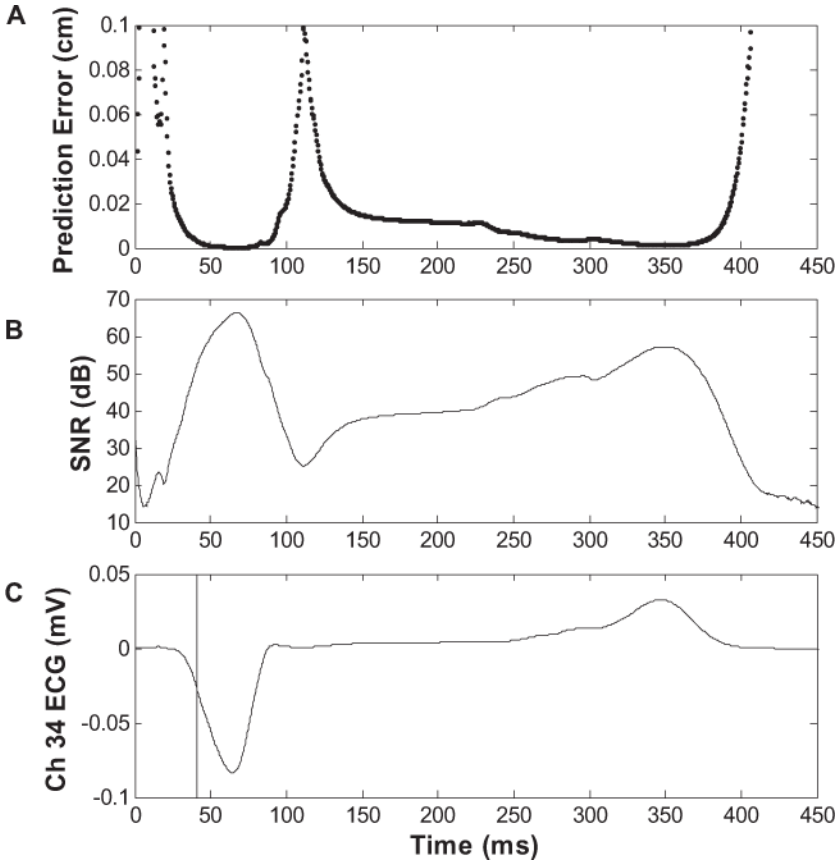

Figure 2.

Representative examples of the prediction error and signal-to-noise ratio during the cardiac cycle. (A) Prediction error. (B) Signal-to-noise ratio (SNR). (C) ECG signal. Time zero corresponds to the end of the pacing pulse. The vertical line in panel (C) indicates the earliest activation time.

NIH-PA Author Manuscript

NIH-PA Author Manuscript

NIH-PA Author Manuscript

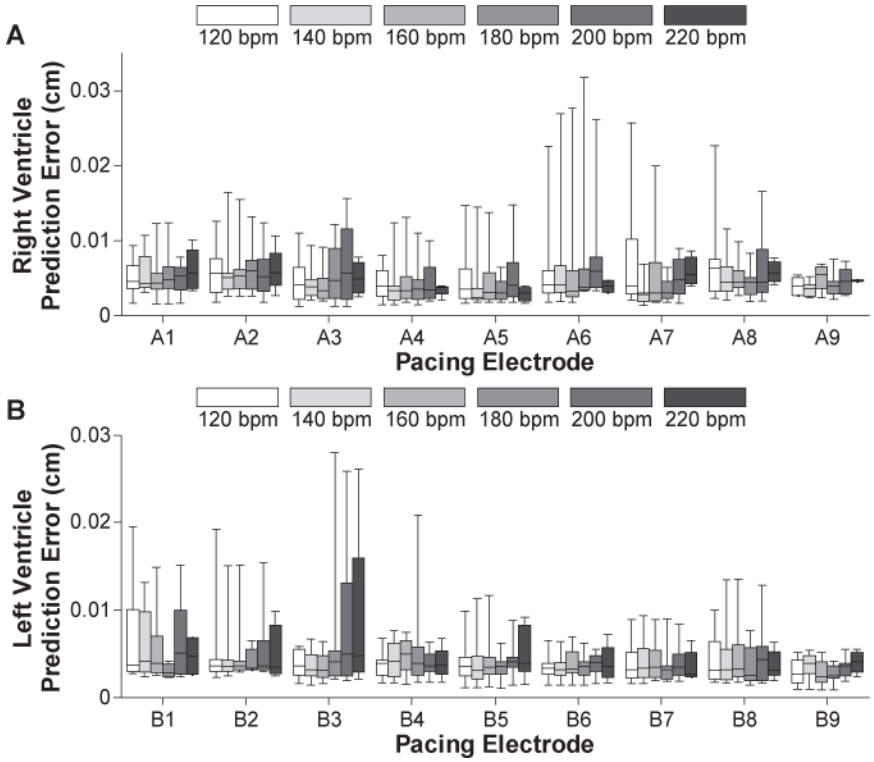

Figure 3.

Prediction errors at the earliest activation time. Results from pacing sites at the right ventricle (A1–A9) and at the left ventricle (B1–B9) are presented at the first and the second entries, respectively. At each pacing electrodes, the prediction errors at six different heart rates are displayed at six separate bars. For each intervention, the five bars at each bar-graph indicate the 5%, 25%, 50%, 75%, and 95% of the distribution.

NIH-PA Author Manuscript

NIH-PA Author Manuscript

NIH-PA Author Manuscript

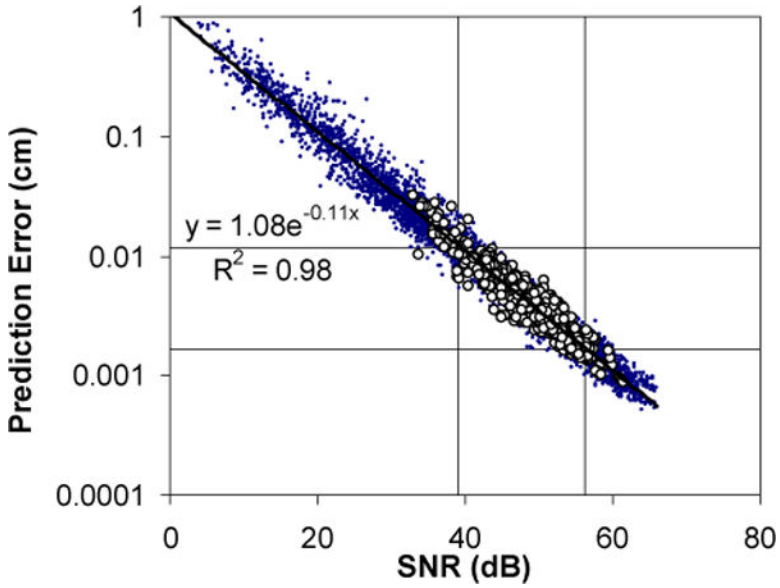

Figure 4.

Prediction error versus signal-to-noise ratio (SNR). Each dot represents SNR and prediction error for solutions ranging from 4 ms after the pacing spike to the time of QRS peak. Especially, values at the earliest activation time (EAT) are represented by empty circles. This plot includes data from all hearts, all heart rates, and all pacing electrodes. The two horizontal and two vertical lines indicate 5% and 95% values of EAT prediction error and SNR, respectively. The y-axis is in logarithmic scale.

NIH-PA Author Manuscript
NIH-PA Author Manuscript
NIH-PA Author Manuscript

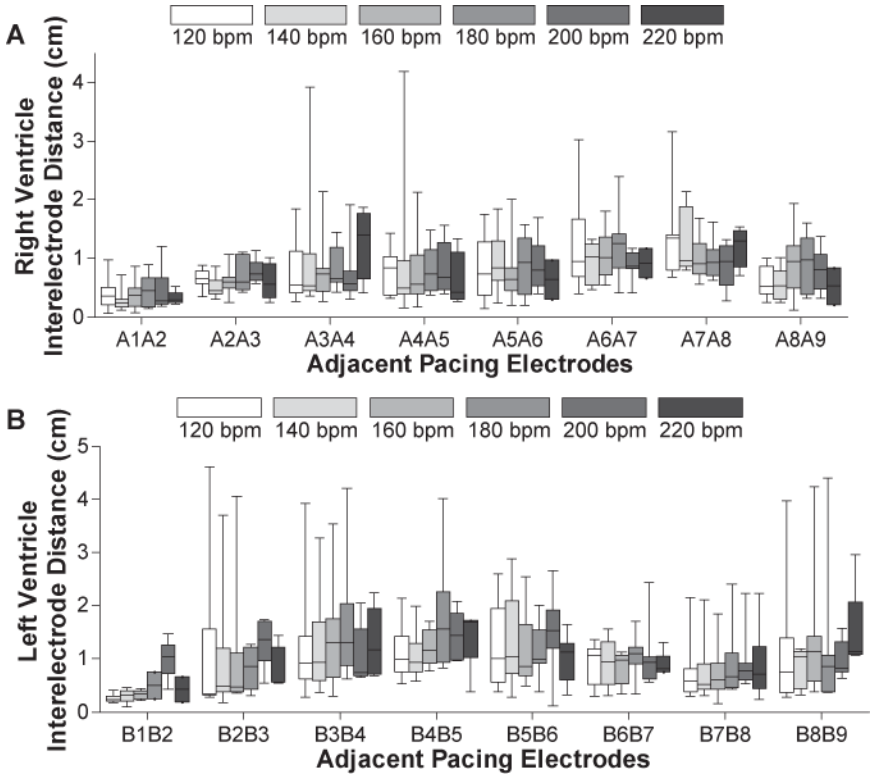

Figure 5.

Distance between adjacent epicardial pacing electrodes. Results from pacing sites at the right ventricle (A1–A9) and at the left ventricle (B1–B9) are presented at the first and the second entries, respectively. At each electrode, the distances at different heart rates are displayed separately. For each intervention, the five bars at each bar-graph indicate the 5%, 25%, 50%, 75%, and 95% of the distribution. The real distances between A1 and A2 (A1A2) and B1 and B2 (B1B2) are 0.2 cm, and all others are 1.0 cm.

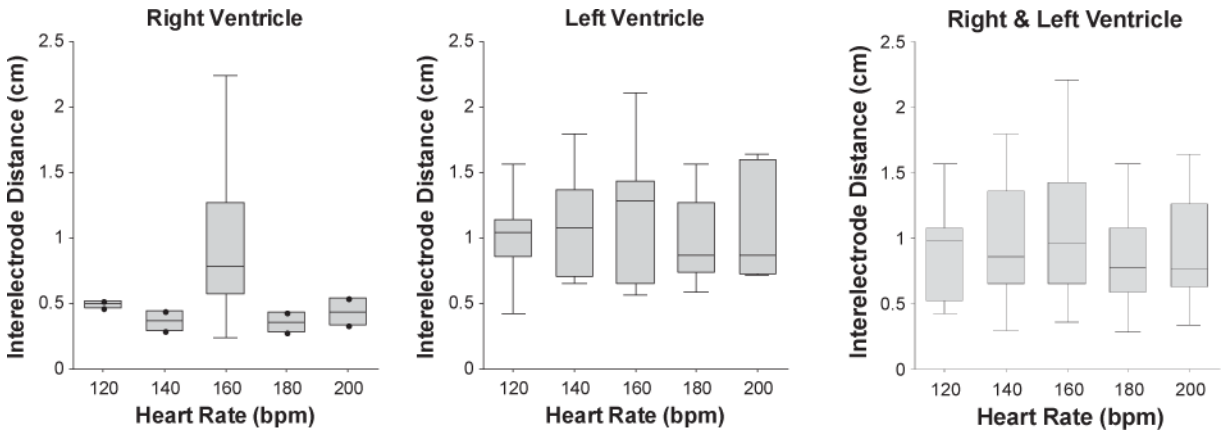

Figure 6.

Distance between adjacent endocardial pacing electrodes. Results from right ventricle, left ventricle, and both ventricles combined are presented at different heart rates. The five bars at each bar-graph indicate the 5%, 25%, 50%, 75%, and 95% of the distribution. The actual interelelectrode distance is 1.2 cm.

NIH-PA Author Manuscript
NIH-PA Author Manuscript
NIH-PA Author Manuscript

NIH-PA Author Manuscript

NIH-PA Author Manuscript

NIH-PA Author Manuscript

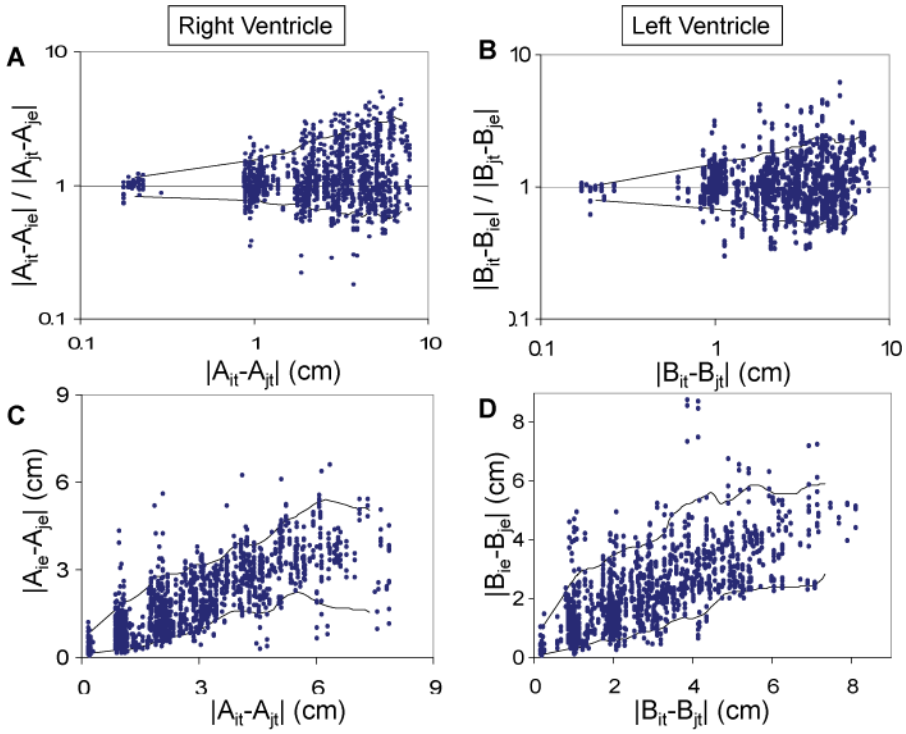

Figure 7.

Estimation of relative and absolute errors. The absolute error between ith and jth electrodes (A_i & A_j or B_i & B_j, $i \neq j$) is defined as the estimated distance between the two electrodes ($|A_{ie}–A_{je}|$ or $|B_{ie}–B_{je}|$; subscript "e" indicates estimated location). The relative error between two electrodes is defined as the ith electrode localization error ($|A_{it}–A_{ie}|$ or $|B_{it}–B_{ie}|$, subscript "t" indicates true location) divided by the jth electrode localization error ($|A_{jt}–A_{je}|$ or $|B_{jt}–B_{je}|$). The x-axis of each plot is the true distance between two electrodes. Each dot indicates values calculated from ith and jth ($i \neq j$) pacing electrodes. All hearts at all beat rates are included. Two solid lines at each plot represent 5% and 95% of y-axis values.

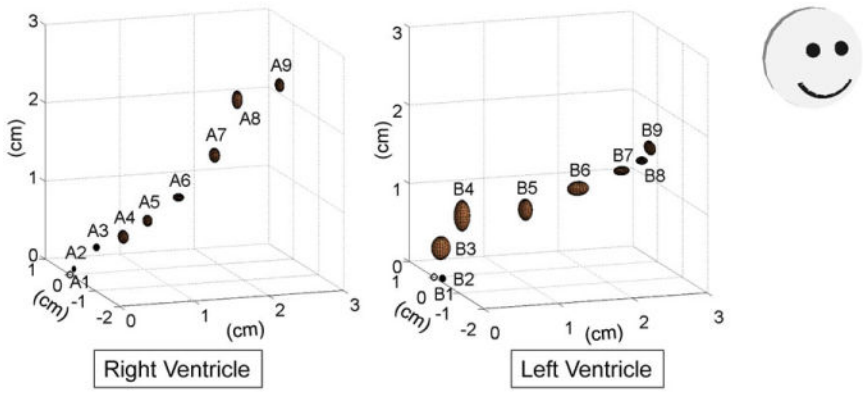

Figure 8.

Three-dimensional distribution of the estimated pacing electrode locations. A1–A9 (B1–B9) indicate nine pacing electrodes on the right (left) anterior ventricular epicardium. The estimation is based on the estimated pacing electrode locations of all the tested hearts. Each estimated pacing site is expressed as an ellipsoid, whose center is the median and each x, y, and z semiaxis represents standard error in the direction. The first pacing site (A1 or B1) is the origin and indicated by an empty circle. The ellipsoid of A2 (B2) is determined by the relative estimated locations of A2 (B2) to A1 (B1) of all the tested hearts. In the same way, the A3 (B3) ellipsoid is determined by the relative locations of A3 (B3) to A2 (B2), and so on.

NIH-PA Author Manuscript NIH-PA Author Manuscript NIH-PA Author Manuscript